Hindawi
International Journal of Antennas and Propagation
Volume 2020, Article ID 3984148, 9 pages
https://doi.org/10.1155/2020/3984148

Research Article

Space-Time Correlation for Three-Dimensional MIMO Channel Model Using Leaky Coaxial Cables in Rectangular Tunnel

Kai Zhang, Fangqi Zhang, and Guoxin Zheng

Key Laboratory of Specialty Fiber Optics and Optical Access Networks, Shanghai University, 99 Shangda Road, Shanghai 200444, China

Correspondence should be addressed to Guoxin Zheng; gxzheng@staff.shu.edu.cn

Received 19 June 2020; Revised 27 July 2020; Accepted 4 August 2020; Published 20 August 2020

Academic Editor: Ana Alejos

The rapid development of high-speed train and Metro communications has provided new challenges for the application of MIMO technologies. Therefore, we propose a three-dimensional (3D) multiple-input multiple-output (MIMO) channel model using leaky coaxial cable (LCX) in a rectangular tunnel. The channel model is based on geometry-based single-bounce (GBSB) channel model and the electric field distribution of LCX in the tunnel environment. The theoretical expressions of channel impulse response (CIR) and space-time correlation function (CF) are also derived and analyzed. The CFs for different model parameters (moving velocity and moving time) and different regions of the tunnel are simulated by Monte Carlo method to verify the theoretical derivation at 1.8 GHz. In the same parametric configuration of nonstationary tunnel scenarios, the time delay of the first minimum value of CFs for LCX-MIMO is 1/5 of the time delay of the minimum value of CFs for dipole antennas MIMO when the train moving velocity is 360 km/h. It is shown that, for MIMO system, the performance of using LCXs is better than using dipole antennas.

1. Introduction

Recently, multiple-input multiple-output (MIMO) technology has been widely used in many scenarios. The nonstationary scenarios of MIMO technologies for high-speed train and Metro communications have drawn attention. Up to present, there are two main cases of nonstationary scenarios: one is the movement of transmitter or receiver and the other is the movement of transmitter and receiver [1–12]. The channel modeling can be based on two-dimensional (2D) [1–5] and three-dimensional (3D) [6–12]. According to the 3GPP (3GPP TR 25.996) spatial channel model (SCM) [1–6] and WINNER II channel model [7–12], the geometry-based single-bounce (GBSB) [1–5] and geometry-based stochastic model (GBSM) [6–12] are used to describe MIMO propagation channels. The nonstationary scenarios investigated include the high altitude unmanned aerial vehicles (UAV) MIMO air-to-ground communications [7, 8], the vehicle-to-vehicle communications in tunnel [9, 10] and other scattering environments [11, 12], the base-station-to-vehicle communications in tunnel [5] and other scattering environments [1, 2], and so on. In these scenarios, the influences of different moving velocities, moving times, moving directions, and moving trajectories on spatial cross-correlation and auto-correlation are analyzed [6–12]. In [1, 2], the authors have researched the multielement antennas systems in mobile fading channels and have considered that the local scatterers were only around the mobile user (MS) in 2×2 MIMO channel, the base station (BS) is fixed, the BS and the MS are both two-element antennas array, and they also derived a space-time correlation for MIMO systems in mobile fading channels. It could be called "one-ring" model in physical MIMO channel models. In [4], the authors analyzed the propagation characteristics of mobile-to-mobile fading channels for MIMO systems; they derived a great channel model in mobile-to-mobile fading channels and scatterers around both transmitting antennas and receiving antennas. It could be called "two-ring" model in physical MIMO channel models. In [9], the authors studied a nonstationary geometry-based channel model for MIMO vehicle-to-vehicle communications in tunnel environments and derived the theoretical expressions of channel impulse response and spatial

correlation functions (SCFs), and they discussed the SCFs for different time delay, different receiving antenna spacing, and different frequency separation. In [11], this paper researched a geometry-based nonstationary MIMO channel model for vehicular communications and discussed the autocorrelation functions (ACFs) for different time separation and different receiving antenna spacing. In [12], this paper proposed a 3D wideband nonstationary multimobility model for vehicle-to-vehicle MIMO channels and derived the channel impulse response (CIR) and correlation functions (CFs); the authors discussed the CFs for different time separations and different times which increased with the increase of time separation and time by simulation.

At the moment, there are some shortcomings in the study of confined area communication such as subway tunnels. Leaky coaxial cable (LCX) is usually used as an antenna (the input signal is entered from single port of every single LCX) and two antennas (the input signal is entered from double ports of every single LCX) to transmit signals in tunnel, due to uniform radiation. Most of the researches on the application of LCX are focused on the measurement and analysis in tunnel and linear-cell environments [13, 14]. In [13], the authors present a 2×2 MIMO measurement campaign using LCX in tunnel environment at 1.8 GHz, and the results of capacity and condition number indicate that the MIMO performance is not highly dependent on the LCX spacing. In [14], the authors used single LCX as two antennas and researched propagation characteristics of the LCX-MIMO systems in linear-cell environment at 2.4 GHz and 5 GHz, and the capacity results indicate that the LCX-MIMO can achieve more capacity improvement than that of channel using monopole antennas with the simple equal power allocation. A few of them have carried out theoretical description. The channel models of these researches are stationary [15]. In [15], the authors research the theoretical channel model of 2-by-2 MIMO system using single LCX in free space, and the results show that a 2-by-2 MIMO system can achieve good performance using single LCX. In [16], the authors proposed a GBSB model for MIMO channel using LCXs in tunnel based on the electric field distribution of the LCX and analyzed the performance of MIMO system in terms of capacity, condition number (CN), and CF by simulation and measurement. But in [16], the authors only studied the stationary scenario. There is little research on nonstationary LCX-MIMO communication in tunnel scenarios. With the rapid development of Metro and high-speed railway, there is an urgent need for the study of LCX-MIMO in nonstationary tunnel scenarios.

For high-speed railway scenario and Metro scenario, this paper aims to fill these research gaps. We propose a 3D nonstationary LCX-MIMO channel model in rectangular tunnel environments. The main contributions and novelties of this paper are summarized as follows: (1) this paper develops a 3D nonstationary LCX-MIMO channel model, and the channel impulse response (CIR) and spatial correlation function (CF) are theoretically derived. The proposed model is verified by comparing the spatial CF theory with simulation; (2) this model considers the influence of the receiver's mobility on the propagation characteristic of LCX-MIMO system, in terms of the moving velocity and moving time. The influence of the different positions where the receiver is located in the tunnel on the propagation characteristics is also analyzed; (3) the CFs of LCX-MIMO and dipoles MIMO are compared with different moving velocities for different time delays.

The remainder of this paper is organized as follows. In Section 2, we propose a 3D nonstationary LCX-MIMO channel model. In Section 3, the theoretical expressions of space-time CF for our proposed GBSB 3D nonstationary in tunnel scenarios are derived. In Section 4, the space-time CFs of the proposed model are simulated and validated. Finally, our concluding remarks are given in Section 5.

2. 3D Nonstationary LCX-MIMO Channel Model

Figure 1(a) shows the LCX structure; Figure 1(b) shows LCXs (transmitter, Tx) and dipoles (receiver, Rx) installation; and Figure 1(c) shows the 2-by-2 nonstationary LCX-MIMO transmission system in rectangular tunnel environments and the input signals of LCXs are s_1 and s_2. In Figure 1, the O is origin of the coordinate; the parallel direction to axis of tunnel presents the Z-axis of the coordinate system; the cross section of tunnel presents the XOY-plane, the vertical direction of the XOY-plane presents the Y-axis of the coordinate system, and the horizontal direction of the XOY plane presents the X-axis of the coordinate system. In Figure 2, for the MIMO system, the parameter names and symbols of LCX-MIMO channel model are as shown in Table 1.

In this paper, we only consider LCX with vertical periodic slots, the length of LCX is L, the periodic of slot of LCX is P, and the number of slots of LCX is N. According to the electromagnetic field theory of antenna, the slots of LCX can be seen as a series of magnetic dipoles, and the electric field distribution of a single slot E_z can be expressed as [17, 18]

$$E_z = E_0 \frac{e^{-jk_0 r}}{r} \sin(\theta), \tag{1}$$

where E_0 denotes the electric field strength of the slot surface, r denotes the distance from a point in the electric field of LCX to a slot, θ is the angle between the direction of r and the axial direction of LCX, $k_0 = 2\pi f/c$ denotes the propagation constant in free space, f is the center frequency, and c is velocity of light.

The longitudinal amplitude attenuation of i-th slot of LCX α_i, phase variation i-th slot of LCX β_i, and the propagation constant k_r in LCX are as follows:

$$\alpha_i = \alpha_0^i, \tag{2a}$$

$$\beta_i = \beta_0 i, \tag{2b}$$

$$k_r = k_0 \sqrt{\varepsilon_r}, \tag{2c}$$

where α_0 is amplitude attenuation of LCX per slot, $\beta_0 = k_r P$ is phase variation of LCX per slot, and $\square_r$ is the dielectric constant of LCX.

Because of the rough surface of the tunnel wall, it can be considered that there exists diffuse reflection of electromagnetic wave from the transmitter to the receiver in the

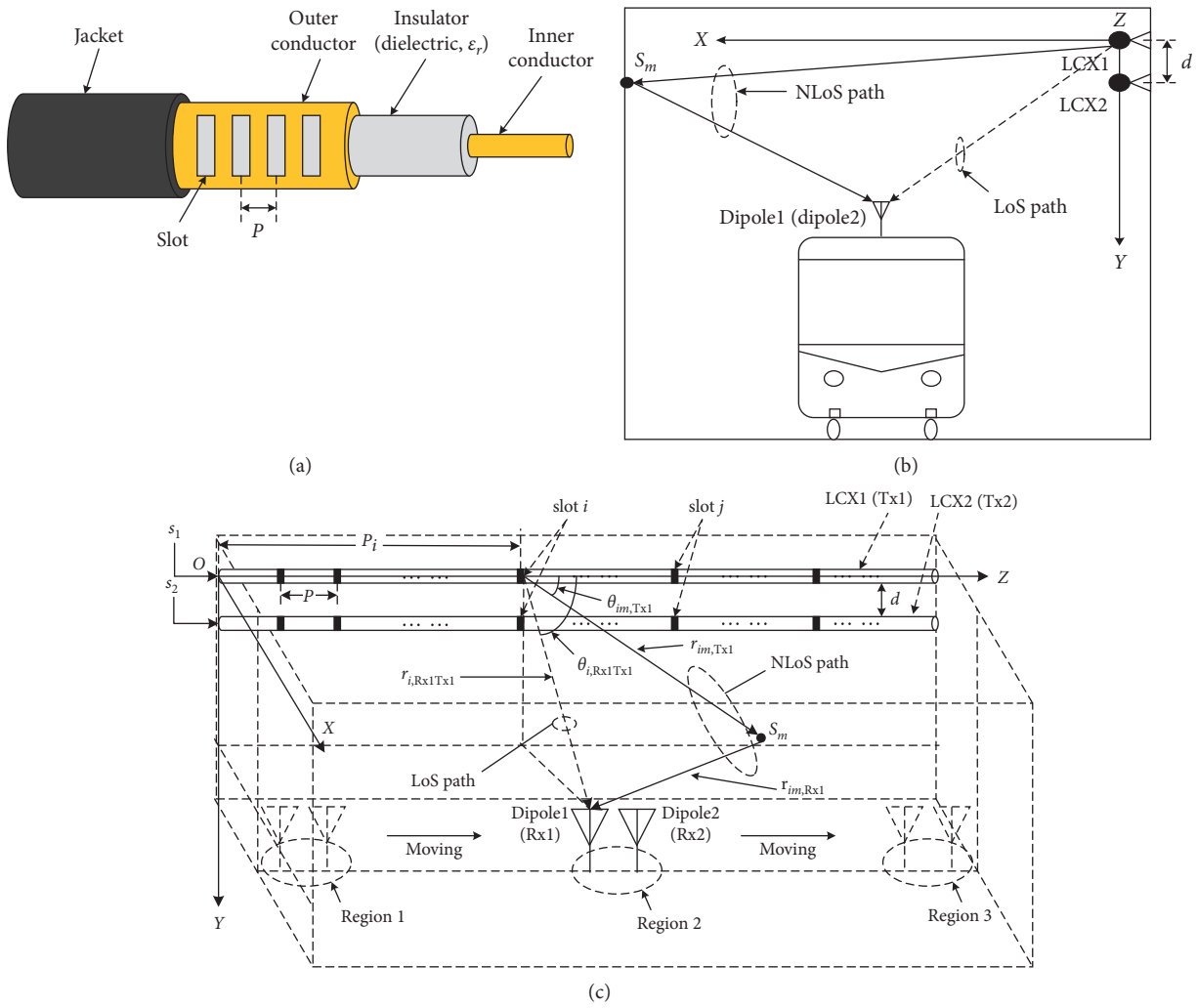

Figure 1: (a) LCX structure; (b) LCXs and dipoles installation; (c) signal propagation for LoS and NLoS path of LCX-MIMO transmission scheme.

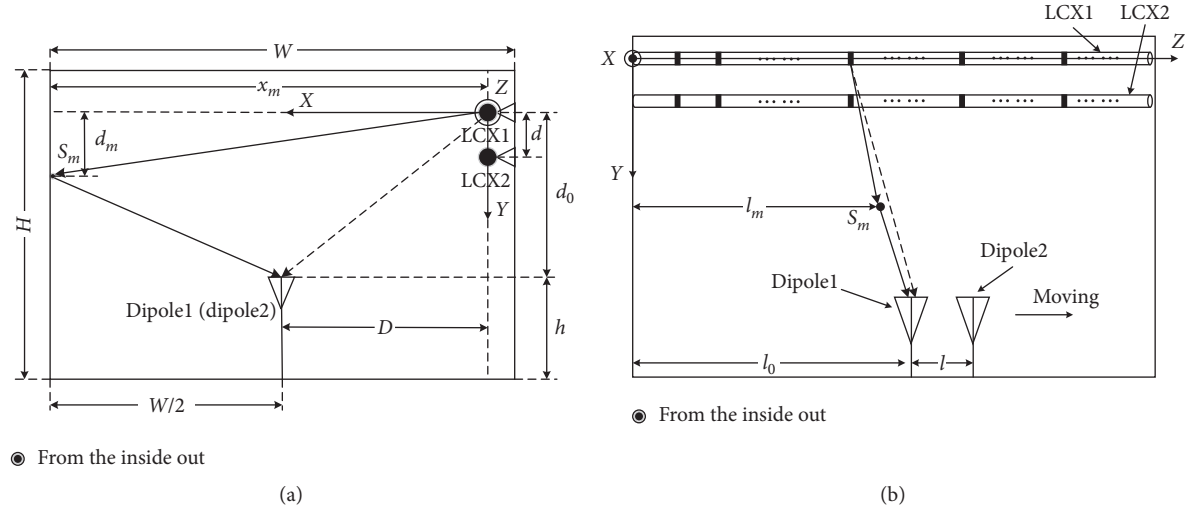

Figure 2: Continued.

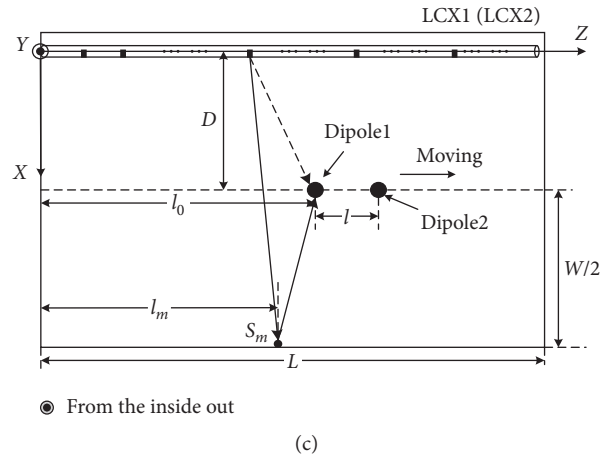

(c)

Figure 2: Projection view of the LCX-MIMO in a rectangular tunnel: (a) the front view; (b) the side view; (c) the top view.

Table 1: Parameters name and symbol of LCX-MIMO channel model.

Name	Symbol
Tunnel size (length × width × height)	$L \times W \times H$
Length of LCX	L
LCX spacing	D
LCX relative permittivity	ε_r
Receiving antennas spacing	l
Coordinate of dipole1 (Rx1)	(D, d_0, l_0)
Period of LCX slot	P
Number of LCX slots	$N = \text{floor}\ (L/P)-1$
Coordinate of m-th of scatterer S_m	(x_m, d_m, l_m)

tunnel, and the number of effective diffuse reflection locations is M. We assumed that the diffuse reflection locations obey uniform distribution, and all the effective diffuse locations are located on the tunnel side wall opposite to LCX. Therefore, the total electric field strength of a certain point in the tunnel can be considered as the vector superposition of LoS and NLoS components as shown in Figure 2. The LoS and NLoS components of electric field distribution from the p-th (p = Tx1, Tx2) LCX to the l-th (l = Rx1, Rx2) receiving antenna can be expressed as [16]

$$E_{z,lp}^{\text{LoS}} = \sum_{i=1}^{N} E_i \frac{e^{-jk_0 r_{i,lp}}}{r_{i,lp}} \sin\left(\theta_{i,lp}\right), \tag{3a}$$

$$E_{z,lp}^{\text{NLoS}} = \sum_{i=1}^{N} \sum_{m=1}^{M} E_i \frac{e^{-jk_0\left(r_{im,p}+r_{im,l}\right)}}{r_{im,p}+r_{im,l}} \sin\left(\theta_{im,p}\right), \tag{3b}$$

where $E_i = E_0 \alpha_i e^{-j\beta i}$ denotes the electric field strength of the i-th slot surface of LCX. E_0 denotes the original electric field strength of LCX (we assume that E_0 equals 1 V/m). $r_{i,lp}$ is the distance from the i-th slot of p-th LCX to the l-th receiving antenna. $r_{im,p}$ and $r_{im,l}$ are the distances from the i-th slot of p-th LCX to m-th ($m = 1,\ldots,M$) effective diffuse point S_m and from m-th effective diffuse point S_m to l-th receiving antenna, respectively. $\theta_{i,lp}$ and $\theta_{im,p}$ are the angles between the direction of $r_{i,lp}$ and the axial direction of LCX and between the direction of $r_{im,p}$ to the axial direction of LCX, respectively.

The LCX-MIMO channel model can be described by 2×2 complex channel impulse response (CIR) matrix, i.e., $\mathbf{H}(t) = [h_{lp}(t)]_{2\times 2}$, where $\Omega_{lp} = E[|h_{lp}(t)|^2]$. The CIR $h_{lp}(t)$ from p-th transmitting antenna (Tx) to l-th receiving antenna (Rx) is a vector superposition of the two components CIR of LoS and NLoS and can be expressed as [16]

$$h_{lp}^{\text{LoS}}(t) = \sqrt{\frac{K_{lp}\Omega_{lp}}{K_{lp}+1}} \lim_{N\longrightarrow\infty} \frac{1}{\sqrt{N}} \sum_{i=1}^{N} G_{i,lp}^{\text{LoS}}(t) e^{-j\left[k_0 r_{i,lp}(t)+\beta_i\right]}, \tag{4a}$$

$$h_{lp}^{\text{NLoS}}(t) = \sqrt{\frac{\Omega_{lp}}{K_{lp}+1}} \lim_{\substack{N\longrightarrow\infty \\ M\longrightarrow\infty}} \frac{1}{\sqrt{NM}} \sum_{i=1}^{N} \sum_{m=1}^{M} G_{im,lp}^{\text{NLoS}}(t) e^{j\left[\varphi_{im}-k_0\left(r_{im,p}+r_{im,l}(t)\right)-\beta_i\right]}, \tag{4b}$$

where φ_{im} denotes the phase shift that follows the random variables uniform distribution in the interval $[0, 2\pi)$ and caused by effective diffuse reflection points in tunnel side wall; K_{lp} denotes Rician factor, i.e., $K_{lp} = |h_{lp}^{\mathrm{LoS}}(t)|^2 / E[|h_{lp}^{\mathrm{NLoS}}(t)|^2]$; $G_{i,lp}^{\mathrm{LoS}}(t)$ and $G_{im,lp}^{\mathrm{NLoS}}(t)$ can be calculated by

$$G_{i,lp}^{\mathrm{LoS}}(t) = \frac{\alpha_i\left(\sin\left[\theta_{i,lp}(t)\right]/r_{i,lp}(t)\right)}{\left\{N^{-1}\sum_{i=1}^{N} E\left[\left(\alpha_i\left(\left(\sin\left[\theta_{i,lp}(t)\right]\right)/\left(r_{i,lp}(t)\right)\right)\right)^2\right]\right\}^{1/2}},$$
$$G_{im,lp}^{\mathrm{NLoS}}(t) = \frac{\alpha_i\left(\sin\left(\theta_{im,p}\right)/\left(r_{im,p} + r_{im,l}(t)\right)\right)}{\left\{(NM)^{-1}\sum_{i=1}^{N}\sum_{m=1}^{M} E\left[\left(\alpha_i\left(\left(\sin\left(\theta_{im,p}\right)\right)/\left(r_{im,p} + r_{im,l}(t)\right)\right)\right)^2\right]\right\}^{1/2}}. \tag{5}$$

The particular representation of $h_{lp}^{\mathrm{LoS}}(t)$ and $h_{lp}^{\mathrm{NLoS}}(t)$ in terms of K_{lp}, together with the assumption of $N^{-1}\sum_{i=1}^{N} E[(G_{i,lp}^{\mathrm{LoS}})^2] \longrightarrow 1$ and $(NM)^{-1}\sum_{i=1}^{N}\sum_{m=1}^{M} E[(G_{im,lp}^{NLoS})^2] \longrightarrow 1$ as $N \longrightarrow \infty$ and $M \longrightarrow \infty$, guarantees that $\Omega_{lp} = E[|h_{lp}(t)|^2]$.

3. Spatial Correlation Function

In order to study the performance of the proposed LCX-MIMO channel model, this paper assumes that the LoS and NLoS components are independent of each other and the values of amplitude of LoS and NLoS CIR are zero-mean processes. According to [1, 2], this paper assumes that the CF of transmitter and the CF of receiver are independent of each other, and the CF of receiver is very small. Therefore, we mainly analyze the spatial CF of LCX at the transmitter, and the spatial CF can be expressed as

$$\begin{aligned}\rho_{Rx1Tx1,Rx1Tx2}(t,\tau) &= \frac{E\left[h_{Rx1Tx1}(t)h_{Rx1Tx2}^{*}(t-\tau)\right]}{\sqrt{\left(E\left[\left|h_{Rx1Tx1}(t)\right|^2\right]\right)\left(E\left[\left|h_{Rx1Tx2}(t-\tau)\right|^2\right]\right)}},\\ &= \frac{E\left[h_{Rx1Tx1}^{\mathrm{LoS}}(t)\left(h_{Rx1Tx2}^{\mathrm{LoS}}(t-\tau)\right)^{*}\right] + E\left[h_{Rx1Tx1}^{\mathrm{NLoS}}(t)\left(h_{Rx1Tx2}^{\mathrm{NLoS}}(t-\tau)\right)^{*}\right]}{\sqrt{\Omega_{Rx1Tx1}\Omega_{Rx1Tx2}}},\\ &= \rho_{Rx1Tx1,Rx1Tx2}^{\mathrm{LoS}}(t,\tau) + \rho_{Rx1Tx1,Rx1Tx2}^{\mathrm{NLoS}}(t,\tau).\end{aligned} \tag{6}$$

According to formulas (4a) and (4b), the spatial CFs of LoS and NLoS can be expressed as

$$\rho_{Rx1Tx1,Rx1Tx2}^{\mathrm{LoS}}(t,\tau) = \sqrt{\frac{K_{Rx1Tx1}K_{Rx1Tx2}}{(K_{Rx1Tx1}+1)(K_{Rx1Tx2}+1)}}$$
$$\lim_{N\longrightarrow\infty}\sum_{i=1}^{N}\frac{\alpha_i^2\left(\left(\sin\left[\theta_{i,Rx1Tx1}(t)\right]\sin\left[\theta_{i,Rx1Tx2}(t-\tau)\right]\right)/\left(r_{i,Rx1Tx1}(t)r_{i,Rx1Tx2}(t-\tau)\right)\right)}{\sqrt{\left[\sum_{i=1}^{N}\left(\alpha_i\left(\sin\left[\theta_{i,Rx1Tx1}(t)\right]/r_{i,Rx1Tx1}(t)\right)\right)^2\right]\left[\sum_{i=1}^{N}\left(\alpha_i\left(\sin\left[\theta_{i,Rx1Tx2}(t-\tau)\right]/r_{i,Rx1Tx2}(t-\tau)\right)\right)^2\right]}\,e^{-jk_0\left[r_{i,Rx1Tx1}(t)-r_{i,Rx1Tx2}(t-\tau)\right]}}, \tag{7a}$$

$$\rho_{Rx1Tx1,Rx1Tx2}^{\mathrm{NLoS}}(t,\tau) = \frac{1}{\sqrt{(K_{Rx1Tx1}+1)(K_{Rx1Tx2}+1)}}$$
$$\lim_{\substack{N\longrightarrow\infty\\ M\longrightarrow\infty}}\sum_{i=1}^{N}\sum_{m=1}^{M}\frac{\alpha_i^2\left(\sin\left(\theta_{im,Tx1}\right)\sin\left(\theta_{im,Tx2}\right)\right)/\left[r_{im,Tx1}+r_{im,Rx1}(t)\right]\left[r_{im,Tx2}+r_{im,Rx1}(t-\tau)\right]}{\sqrt{AB}} \tag{7b}$$
$$e^{-jk_0\left(r_{im,Tx1}-r_{im,Tx2}\right)},$$

Table 2: Simulations parameters.

Name	Value
Tunnel size ($L \times W \times H$)	$100\,\text{m} \times 5\,\text{m} \times 3\,\text{m}$
Length of LCX (Tx)	100 m
LCX relative permittivity (ε_r)	1.25
Receiving antennas spacing (d)	0.5 m
Receiver (Rx)	Dipole antenna (horizontal polarization)
x-coordinate of dipole1 (D)	2.44 m
y-coordinate of dipole1 (d_0)	1.1 m
Period of LCX slot (P)	0.25 m
Number of LCX slots (N)	399
Longitudinal attenuation constant of LCX (α)	4.1 dB/100 m
Frequency (f)	1.8 GHz
Light velocity (c)	3×10^8 m/s
Wave length (λ)	c/f
Region 1	[0 m, 2 m]
Region 2	[49 m, 51 m]
Region 3	[98 m, 100 m]

where $A = \sum_{i=1}^{N} \sum_{m=1}^{N} (\alpha_i \sin(\theta_{im,Tx1})/r_{im,Tx1} + r_{im,Rx1}(t))^2$;
$B = \sum_{i=1}^{N} \sum_{m=1}^{M} (\alpha_i \sin(\theta_{im,Tx2})/r_{im,Tx2} + r_{im,Rx1}(t-\tau))^2$;
$\sin[\theta_{i,Rx1Tx1}(t)] = \sqrt{d_0 + D^2}/r_{i,Rx1Tx1}(t)$;
$\sin[\theta_{i,Rx1Tx2}(t-\tau)] = \sqrt{d_0 + D^2}/r_{i,Rx1Tx2}(t-\tau)$;
$r_{i,Rx1Tx1}(t) = \left\{d_0^2 + [(l_0 - ip) + vt]^2 + D^2\right\}^{1/2}$;
$r_{i,Rx1Tx2}(t) = \left\{(d_0 - d)^2 + [(l_0 - ip) + vt]^2 + D^2\right\}^{1/2}$;
$\sin(\theta_{im,Tx1}) = \sqrt{x_m^2 + d_m^2}/r_{im,Tx1}$;
$\sin(\theta_{im,Tx2}) = \sqrt{x_m^2 + d_m^2}/r_{im,Tx2}$;
$r_{im,Tx1} = \sqrt{(l_m - ip)^2 + d_m^2 + x_m^2}$;
$r_{im,Tx2} = \sqrt{(l_m - ip)^2 + (d_m - d)^2 + x_m^2}$;
$r_{im,Rx1}(t) = \sqrt{(l_0 + vt - l_m)^2 + (d_0 - d_m)^2 + (W/2 - x_m)^2}$.

4. Simulation Results and Discussion

According to formulas (5), (7a), and (7b), the spatial CF (LoS + NLoS) is simulated by Monte Carlo method, because the LoS component of CIR is deterministic, and NLoS component of CIR is random process. So, we can multiple iteration NLoS component of CIR by Monte Carlo method. In this paper, we set the number of iterations to 5×10^4. In this paper, the parameters setup of simulation is mainly a reference to [13]. For the simulation of this paper, we assumed that the LCXs are installed at the tunnel side wall, and the dipole antennas are moving on the axial direction of tunnel ground. K_{11} and K_{12} are set to be of the same values (1 dB, 4 dB, 8 dB, 16 dB). Firstly, the receiver is located in Region 2 of tunnel (i.e., the tunnel's axial [49 m, 51 m], the horizontal distance from the tunnel's side wall to receiver is 2.44 m, and the vertical distance from LCX1 to receiver is $d_0 = 1.1$ m). The influence of different moving velocities (90 km/h, 180 km/h, and 360 km/h) of the receiver, different relative time delays of the two paths, different LCX spacing, and different moving times on spatial CF is analyzed. Meanwhile, the influence of different regions of receiver in tunnel on spatial CF is analyzed by simulation. For all regions, the horizontal distance from the tunnel's side wall to receiver is 2.44 m, and the vertical distance from LCX1 to receiver is $d_0 = 1.1$ m. The other parameters of simulation are presented in Table 2.

Figure 3(a) describes the simulation and theoretical results of spatial CF as the time delay increases at different moving velocities of receiver. Figure 3(b) describes the change of simulation and theoretical spatial CF as the time delay increases when the receiver is moving at different moving times. The results are consistent with those described in [10]. Figure 3(a) shows that the spatial CF decreases with the increasing of moving velocity of the receiver. Figure 3(b) shows that the spatial CF decreases with the increasing of time delay for various times. Figure 3(c) shows that the spatial CF decreases with the increasing of LCX spacing, and it can also be seen that the spatial CF at different locations in the tunnel has little difference. According to Figures 3(a)–3(c), we can see that the theoretical results are consistent with the simulation results, which proves that the theoretical derivation is reasonable and the proposed channel model is reasonable. The amplitude of CF is decreasing when the time delay increases, in Figures 3(a)–3(b). Meanwhile, the longitudinal power attenuation constant of LCX α is 4.1 dB/100 m and there is uniform radiation along the longitudinal direction of the tunnel, so the difference of amplitude of CF is small in the three regions, in Figure 3(c). Figure 4 shows the correlation function (CF) comparison between dipole MIMO (transmitters are changed to two dipoles and located at the same places of LCXs, and only the Z-coordinate of dipoles of transmitters is changed to 50 m) and LCX-MIMO for different velocities with different time delays, and the simulation results indicate that the CFs of LCX-MIMO are less than the CFs of dipoles MIMO at the same parameters configuration of nonstationary tunnel scenarios. Based on the results of Figure 3(c), we can see that there is very little difference in the amplitude of CF of the three regions. So, we only simulated in Region 2 for Figure 4. The time delay of the first minimum value of CFs for LCX-MIMO is 1/5 of the time delay of the minimum value of CFs for dipoles

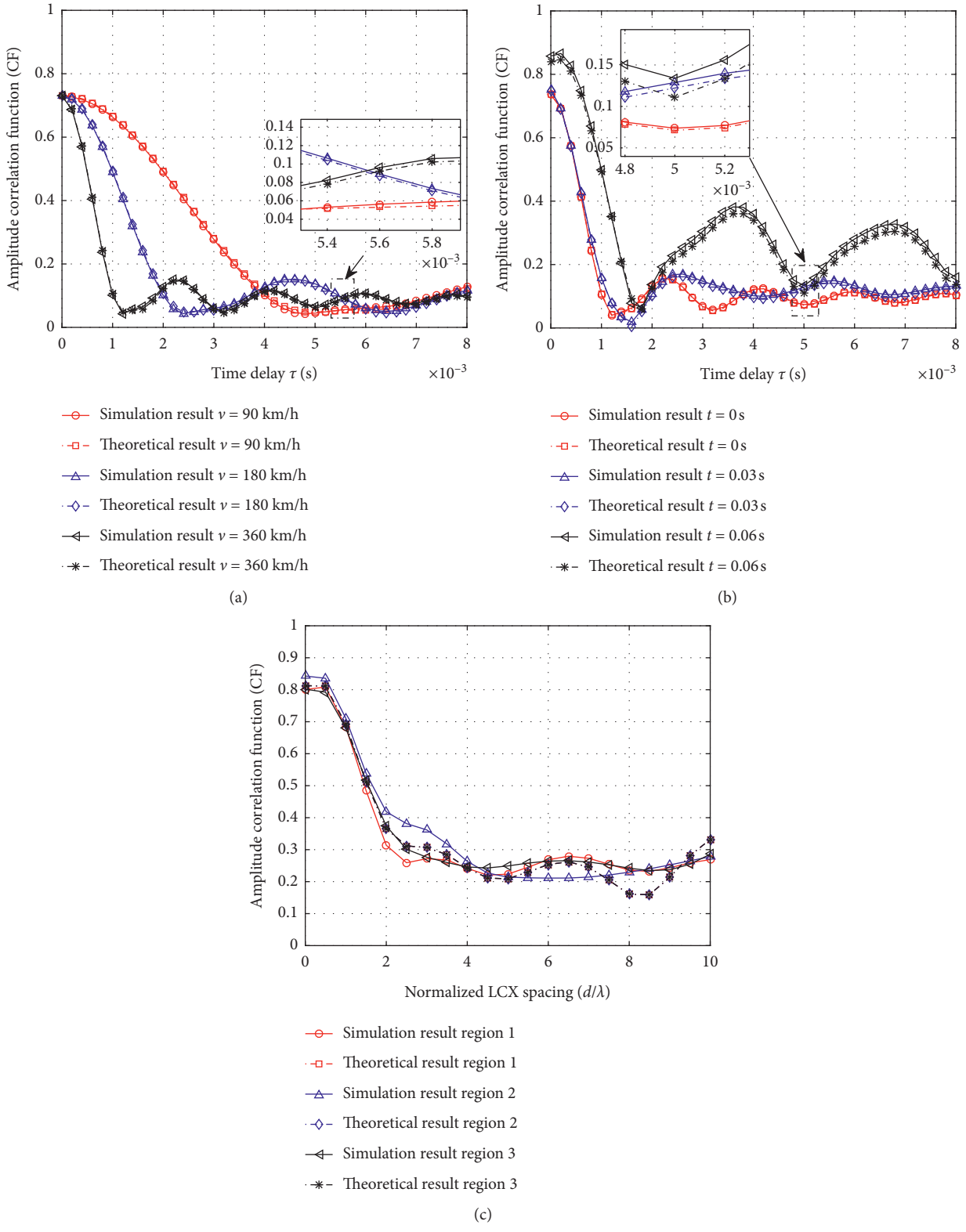

FIGURE 3: Amplitude correlation function (CF: LoS + NLoS): (a) different moving speed and time delay ($t = 0$ s, $d = 0.7\lambda$); (b) different time and time delay ($v = 360$ km/h, $d = 0.7\lambda$); (c) different region Rx1 in tunnel and LCX spacing ($\tau = 0.5$ ms, $t = 0.06$ s, $v = 360$ km/h).

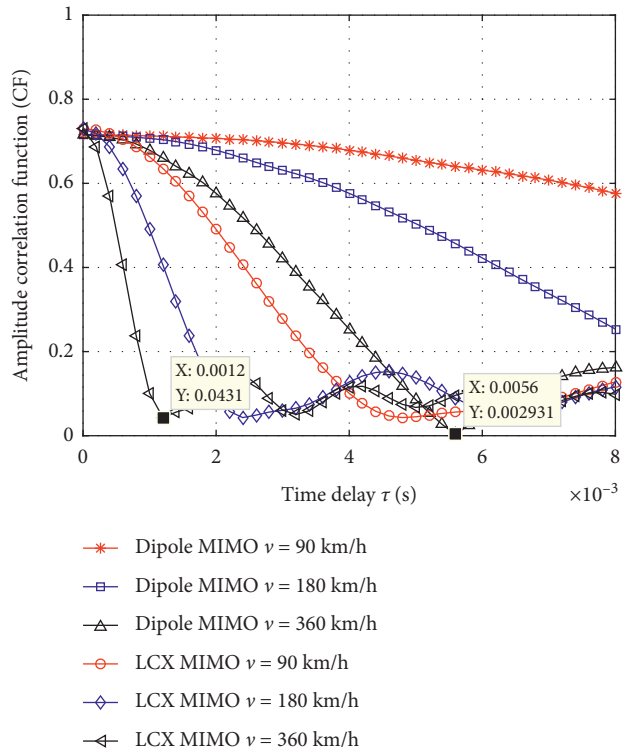

Figure 4: Amplitude correlation function (CF: LoS + NLoS) comparison between dipoles MIMO and LCX-MIMO for different velocity with different time delays ($t = 0$ s, $d = 0.7\lambda$, Region 2).

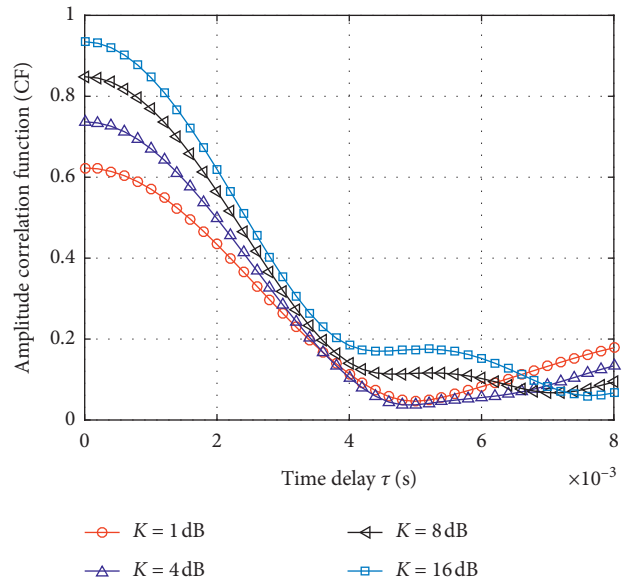

Figure 5: Amplitude correlation function (CF: LoS + NLoS) for different K factors with different time delay ($t = 0$ s, $d = 0.7\lambda$, $v = 90$ km/h).

MIMO when the moving velocity is 360 km/h in Figure 4. In Figure 5, we study the influence of different K factors on CFs with different time delays, and the results show that the CF increases with the increase of the K factor. The multipath component decreases with the increase of the K factor.

5. Conclusion

In this paper, a 3D nonstationary MIMO channel model in rectangular tunnel environment is proposed for Metro and high-speed railway scenarios, the transmitter equipped with two LCXs and the receiver equipped with two dipole antennas, and the receiving antennas array moves along the longitudinal direction of the tunnel. The proposed model and the derived spatial CF expressions are verified by simulation. Comparison of the simulation results and theoretical results indicates that the moving parameters (moving velocity, moving time, and time delay) of the receiver have considerable influences on the LCX-MIMO channel characteristics. The simulation results indicate that the CFs of LCX-MIMO are less than the CFs of dipoles MIMO in the same parameters configuration of nonstationary tunnel scenarios. In the same parametric configuration of nonstationary tunnel scenarios, the time delay of the first minimum value of CFs for LCX-MIMO is 1/5 of the time delay of the minimum value of CFs for dipole antennas MIMO when the train moving velocity is 360 km/h. It is shown that, for MIMO system, the performance of using LCXs is better than using dipole antennas. The simulation results show that the amplitude of CF of the three regions in the tunnel has very little difference.

Data Availability

No data were used to support this study because there are theoretical and simulation results in this paper.

Conflicts of Interest

The authors declare that they have no conflicts of interest.

Acknowledgments

This work was supported by the National Science Foundation of China (Grant nos. 61571282 and 61871261), National Key R&D Program of China (No. 2016YFB1200602), and Fund of Shanghai Cooperative Innovation Center for Maglev and Rail Transit. The authors particularly appreciate Mr. Saleem Asad for his help during writing of this paper.

References

[1] A. Abdi and M. Kaveh, "A space-time correlation model for multielement antenna systems in mobile fading channels," *IEEE Journal on Selected Areas in Communications*, vol. 20, no. 3, pp. 550–560, 2002.

[2] Abdi and M. Kaveh, "Space- time correlation modeling of multielement antenna system in mobile fading channels," in *IEEE International Conference on Acoustics, Speech, and Signal Processing. Proceedings (Cat. No.01CH37221)*, pp. 2505–2508, Salt Lake City, UT, USA, May 2001.

[3] G. J. Byers and F. Takawira, "Spatially and temporally correlated MIMO channels: modeling and capacity analysis,"

IEEE Transactions on Vehicular Technology, vol. 53, no. 3, pp. 634–643, 2004.

[4] M. Patzold, B. Hogstad, and N. Youssef, "Modeling, Analysis, and simulation of MIMO mobile-to-mobile fading channels," *IEEE Transactions on Wireless Communications*, vol. 7, no. 2, pp. 510–520, 2008.

[5] H. D. Zheng and X. Y. Nie, "GBSB model for MIMO channel and its space-time correlation analysis in tunnel," in *Proceedings of the 2008 IEEE International Symposium on Knowledge Acquisition and Modeling Workshop*, pp. 221–224, Wuhan, China, December 2008.

[6] Q. Zhu, Y. Yang, C.-X. Wang et al., "Spatial correlations of a 3-D non-stationary MIMO channel model with 3-D antenna arrays and 3-D arbitrary trajectories," *IEEE Wireless Communications Letters*, vol. 8, no. 2, pp. 512–515, 2019.

[7] H. Jiang, Z. Zhang, L. Wu, and J. Dang, "Three-dimensional geometry-based UAV-MIMO channel modeling for A2G communication environments," *IEEE Communications Letters*, vol. 22, no. 7, pp. 1438–1441, 2018.

[8] X. Cheng and Y. Li, "A 3-D geometry-based stochastic model for UAV-MIMO wideband nonstationary channels," *IEEE Internet of Things Journal*, vol. 6, no. 2, pp. 1654–1662, 2019.

[9] H. Jiang, Z. Zhang, L. Wu, J. Dang, and G. Gui, "A 3-D non-stationary wideband geometry-based channel model for MIMO vehicle-to-vehicle communications in tunnel environments," *IEEE Transactions on Vehicular Technology*, vol. 68, no. 7, pp. 6257–6271, 2019.

[10] N. Avazov, S. M. R. Islam, D. Park, and K. S. Kwak, "Statistical characterization of a 3-D propagation model for V2V channels in rectangular tunnels," *IEEE Antennas and Wireless Propagation Letters*, vol. 16, pp. 2392–2395, 2017.

[11] Y. Ma, L. Yang, and X. Zheng, "A geometry-based non-stationary MIMO channel model for vehicular communications," *China Communications*, vol. 15, no. 7, pp. 30–38, 2018.

[12] J. Bian, C.-X. Wang, J. Huang et al., "A 3D wideband non-stationary multi-mobility model for vehicle-to-vehicle MIMO channels," *IEEE Access*, vol. 7, pp. 32562–32577, 2019.

[13] Y. Wu, G. Zheng, A. Saleem, and Y. P. Zhang, "An experimental study of MIMO performance using leaky coaxial cables in a tunnel," *IEEE Antennas and Wireless Propagation Letters*, vol. 16, pp. 1663–1666, 2017.

[14] Y. Hou, S. Tsukamoto, S. Li, T. Higashino, K. Kobayashi, and M. Okada, "Capacity evaluation of MIMO channel with one leaky coaxial cable used as two antennas over linear-cell environments," *IEEE Transactions on Vehicular Technology*, vol. 66, no. 6, pp. 4636–4646, 2017.

[15] Y. M. Wu, "Performance analysis of MIMO transmission scheme using single leaky coaxial cable," *IEEE Antennas and Wireless Propagation Letters*, vol. 16, pp. 298–301, 2017.

[16] K. Zhang, F. Zhang, G. Zheng, and A. Saleem, "GBSB model for MIMO channel using leaky coaxial cables in tunnel," *IEEE Access*, vol. 7, pp. 67646–67655, 2019.

[17] J. H. Wang and K. K. Mei, "Theory and analysis of leaky coaxial cables with periodic slots," *IEEE Transactions on Antennas and Propagation*, vol. 49, no. 12, pp. 1723–1732, 2001.

[18] L. Shu, J. Wang, H. Shi et al., "Research on the radiation characteristics of the leaky coaxial cables," in *Proceedings of the 6th International SYmposium on Antennas, Propagation and EM Theory, 2003*, pp. 242–245, Beijing, China, October 2003.